Complex Permittivity Model for Time Domain Reflectometry Soil Water Content Sensing: I. Theory

R. C. Schwartz*
S. R. Evett
USDA-ARS
Conservation and Production Research Lab.
Bushland, TX 79012

M. G. Pelletier
USDA-ARS
Cropping Systems Research Lab.
Lubbock, TX 79403

J. M. Bell
USDA-ARS
Conservation and Production Research Lab.
Bushland, TX 79012

Despite numerous applications of time-domain reflectometry (TDR), serious difficulties remain in estimating accurate soil water contents under field conditions, especially in fine-textured soils. We developed a physically based calibration model to predict the frequency- and temperature-dependent complex dielectric response of soils. The model was used to predict frequency-dependent attenuation and a single "effective" frequency approximation of apparent permittivity of the soil. Effective frequency was predicted to decline from 450 to 160 MHz as water contents increased from air dry to saturation. Predicted frequency decline was small for an input bandwidth of 130 MHz, reflecting that modeled polarization mechanisms associated with relaxation frequencies above 100 MHz were responsible for most of the frequency-dependent attenuation. For specific surface areas ranging from 150 to 300 $m^2\ g^{-1}$, simulations indicate that ignoring dielectric and conductive losses or the associated decline in effective frequency results in a 5 to 22% underestimation of the apparent permittivity. Both the power-law and de Loor–Dobson mixing models gave a reasonable approximation to the measured apparent permittivity for a silty clay loam (34% clay) across the entire water content range. Moreover, the models were able to describe the behavior of apparent permittivity in response to temperature for two soils with contrasting bulk electrical conductivity contributions to losses. These results demonstrate that loss mechanisms and declines in effective frequency need to be considered to accurately predict the soil water content of fine-textured soils.

Abbreviations: dc, direct current; PDF, probability density function; TDR, time domain reflectometry.

Time-domain reflectometry has become an established technique to monitor soil water content and has been widely adopted primarily for research applications where in situ measurements are required over short time intervals. In this method, volumetric water content, θ ($m^3\ m^{-3}$), is inferred from the phase velocity of an electromagnetic pulse traveling through a transmission wire in contact with the soil (Topp et al., 1980). Despite numerous applications of TDR and commercially available instrumentation, serious difficulties in estimating accurate soil water contents under field conditions remain, especially in fine-textured soils. The magnitude of apparent permittivity, which is directly related to the measured travel time, is dependent on the bulk electrical conductivity, σ_0 ($S\ m^{-1}$), as well as several polarization mechanisms including bulk water, all of which are temperature dependent. Oscillations of TDR-inferred θ of up to 0.04 $m^3\ m^{-3}$ can result from diel temperature fluctuations in the field (Or and Wraith, 1999). Moreover, θ estimated from broadband dielectric measurements can exhibit temperature sensitivities inconsistent with that expected for bulk water. Based on previous studies, these temperature responses are thought to be principally controlled by the interplay among the temperature dependencies of the static permittivity of bulk water and the volumetric fraction of bound water (Or and Wraith, 1999; Wraith and Or, 1999), as well as the temperature dependence of the bulk electrical conductivity (Evett et al., 2005).

Signal attenuation during propagation of the broadband pulse through the coaxial cable and other connected hardware, as well as through a lossy soil, can cause a shift in the effective bandwidth and consequently change the dielectric response in dispersive media (Hook and Livingston, 1995; Logsdon, 2000; Topp et al., 2000; Robinson et al., 2003). Topp et al. (2000) used a rise-time measurement obtained from the reflection at the TDR rod termination to approximate an effective bandwidth and total losses. In addition, they measured σ_0 independently to estimate (by subtraction of the high-frequency conductivity term from total losses) the dielectric polarization losses, and thence the loss tangent associated with the measured bandwidth. Topp et al. (2000) concluded that both dielectric damping and conductive losses resulting, in part, from the effects of clays had a measurable effect on the real part of permittivity.

The use of dielectric mixing models for soil permits the establishment of a direct relationship between soil physical properties

The mention of trade names of commercial products in this article is solely for the purpose of providing specific information and does not imply recommendation or endorsement by the USDA.

Soil Sci. Soc. Am. J. 73:886-897
doi:10.2136/sssaj2008-0194
Received 3 June 2008.
*Corresponding author (robert.schwartz@ars.usda.gov).
© Soil Science Society of America
677 S. Segoe Rd. Madison WI 53711 USA
All rights reserved. No part of this periodical may be reproduced or transmitted in any form or by any means, electronic or mechanical, including photocopying, recording, or any information storage and retrieval system, without permission in writing from the publisher. Permission for printing and for reprinting the material contained herein has been obtained by the publisher.

and the aggregate dielectric response of the soil constituents, namely soil particles, water, and air. The use of a four-component mixing model that includes the fraction of bound water associated with high-surface-area clays has resulted in improved prediction of the dielectric response of soils (Dobson et al., 1985). In practice, most mixing models developed for soils have omitted the imaginary contributions of some or all of the dielectric damping mechanisms associated with bound and bulk soil water (Dobson et al., 1985; Roth et al., 1990; Dirksen and Dasberg, 1993; Heimovaara et al., 1994; Or and Wraith, 1999). More recently, Boyarskii et al. (2002) and Mironov et al. (2004) described dielectric models of soils for remote microwave applications that include both the real and imaginary components of bound and bulk water. Boyarskii et al. (2002) used an empirical fit to measured data to approximate bound water relaxation times as a function of water film thickness. This permitted the calculation of the complex permittivity of the bound water component based on the Debye formula. In contrast, Mironov et al. (2004) developed soil-specific spectroscopic parameters derived from empirical piecewise fits of the refractive index and normalized attenuation coefficient. Application of the generalized refractive mixing dielectric model of Mironov et al. (2004) requires network analyzer measurements of soils across a range of water contents and at two frequencies. The models of Boyarskii et al. (2002) and Mironov et al. (2004) were developed as single-frequency approximations for the high (1–18 GHz) frequency range and do not consider temperature effects on the dielectric response. This limits the models for use in broadband TDR applications, especially under field conditions where temperature fluctuations are significant.

Detailed spectroscopy studies of mineral soil water systems show that the imaginary part of the complex dielectric permittivity related to bound water (after the removal of direct current conductivity effects) exhibits broadly distributed polarization mechanisms that are still significant at ~0.5 GHz (Ishida et al., 2000; Logsdon, 2000). Dielectric damping resulting from bound water polarization within the TDR frequency range has the potential to decrease the phase velocity not only by a direct increase in the loss tangent, but also through frequency-dependent attenuation, which results in a narrowing of the signal bandwidth. Consequently, we reason that a dielectric mixing model should use temperature-dependent complex permittivities for both the bound and bulk water fractions to have general application for a range of soils and environments.

The overall goal of this study was to develop a practical model and framework to allow temperature- and frequency-dependent water content calibrations in fine-textured soils for the interpretation of routine TDR measurements in the field. The specific objectives of this study were to: (i) develop a physically based model to predict the frequency- and temperature-dependent complex dielectric response of soils; (ii) use the model to predict frequency-dependent attenuation and a single "effective" frequency approximation of apparent permittivity of the soil; and (iii) evaluate the model using data from Schwartz et al. (2009) and other pertinent studies.

THEORY

The apparent permittivity, K_a, of a bulk soil inferred from the propagation (phase) velocity, v_p, of a transverse electromagnetic signal relative to the speed of light, c, can be described as (von Hippel, 1954)

$$K_a = \left(\frac{c}{v_p}\right)^2 = \frac{\varepsilon'(\omega,T)}{2}\left(1+\sqrt{\tan^2\delta+1}\right) \qquad [1]$$

where tan δ is the loss tangent corresponding to the electric phase angle and ε′ is the real component of the relative dielectric permittivity.[1] The frequency- and temperature-dependent complex permittivity ε* of an isotropic material subject to both polarization and direct current (dc) conductivity effects in a sinusoidal electrical field is

$$\varepsilon^*(\omega,T) = \varepsilon'(\omega,T) - j\varepsilon''(\omega,T) - j\frac{\sigma_0(T)}{\omega\varepsilon_0} \qquad [2]$$

where ε″ is the imaginary component of dielectric permittivity related to dielectric damping, ω is angular frequency (rad s^{-1}), T is temperature (K), σ_0 is the dc bulk electrical conductivity (S m^{-1}), ε_0 is vacuum electric permittivity (8.854×10^{-12} F m^{-1}), and $j = \sqrt{-1}$. The loss tangent is defined as the ratio of the imaginary components to the real part of the complex permittivity, given by

$$\tan\delta = \frac{\varepsilon''(\omega,T) + \left[\sigma_0(T)/\omega\varepsilon_0\right]}{\varepsilon'(\omega,T)} \qquad [3]$$

In Eq. [2], the real and imaginary components related to polarization can be estimated using mixing models, whereas σ_0 can be evaluated using TDR by measuring signal attenuation at long times. Treating σ_0 as an aggregate effect (Topp et al., 2000) rather than within a mixing model avoids the difficulties associated with separating out conductive effects with respect to the volume fractions of the solution and soil and their respective contributions to electrochemical interactions at particle–solution interfaces (Saarenketo, 1998; Logsdon and Laird, 2004).

Dielectric Mixing of Volumetric Fractions

The contribution of dielectric polarization, $\varepsilon'(\omega) - j\varepsilon''(\omega)$, to the complex permittivity of a composite medium with one or more relaxation processes can be approximated using dielectric mixing models. We use a four-component dielectric mixing model to estimate both ε″ and ε′ in Eq. [2] with a knowledge of the volumetric fractions of air, soil particles, free water, and water bound to or adsorbed by the surfaces of the soil particles. Substitution of the power-law approximation (Birchak et al., 1974; Dobson et al., 1985; Dirksen and Dasberg, 1993) for $\varepsilon'(\omega) - j\varepsilon''(\omega)$ in Eq. [2] yields the frequency-dependent complex dielectric permittivity:

$$\varepsilon^*(\omega,T) = \left\{\begin{array}{l}\left(1-\frac{\rho_b}{\rho_s}-\theta\right)(\varepsilon_a)^a + \frac{\rho_b}{\rho_s}(\varepsilon_s)^a + \\ (\theta-\theta_{bw})\left[\varepsilon_{fw}^*(\omega,T)\right]^a + \\ \theta_{bw}\left[\varepsilon_{bw}^*(\omega,T)\right]^a\end{array}\right\}^{1/a} - j\frac{\sigma_0}{\omega\varepsilon_0} \qquad [4]$$

[1]We use ε without the r subscript for relative permittivity. All permittivities used here are relative to the permittivity of free space. This convention was necessary to avoid overcomplicated subscript notation for the permittivities of the various soil phases.

where ε_a is gas-phase permittivity, ε_s is solid-phase permittivity, $\varepsilon_{fw}^*(\omega,T)$ is bulk (free) water complex permittivity, $\varepsilon_{bw}^*(\omega,T)$ is bound water complex permittivity, ρ_b is the soil bulk density (kg m^{-3}), ρ_s is particle density (kg m^{-3}), θ_{bw} is the volume fraction of bound water (m^3 m^{-3}), and a is a fitted empirical exponent. We also consider the four-component dielectric mixing model of de Loor (1968), which assumes soil to be represented by an isotropic mixture of plate-like particles, here written as (Dobson et al., 1985)

$$\varepsilon^*(\omega,T)=\frac{3\varepsilon_s+2(\theta-\theta_{bw})[\varepsilon_{fw}^*(\omega,T)-\varepsilon_s]+2\theta_{bw}[\varepsilon_{bw}^*(\omega,T)-\varepsilon_s]+2\left(1-\frac{\rho_b}{\rho_s}-\theta\right)(\varepsilon_a-\varepsilon_s)}{3+(\theta-\theta_{bw})\left[\frac{\varepsilon_s}{\varepsilon_{fw}^*(\omega,T)}-1\right]+\theta_{bw}\left[\frac{\varepsilon_s}{\varepsilon_{bw}^*(\omega,T)}-1\right]+\left(1-\frac{\rho_b}{\rho_s}-\theta\right)\left(\frac{\varepsilon_s}{\varepsilon_a}-1\right)}-j\frac{\sigma_0}{\omega\varepsilon_0} \quad [5]$$

and hereafter referred to as the de Loor–Dobson dielectric mixing model. In both mixing models, bulk and bound water complex permittivity can be described using the Debye or modified forms of the Debye relaxation equation. Apparent permittivity K_a in Eq. [1] can then be evaluated with $\varepsilon'(\omega,T) = \mathrm{Re}(\varepsilon^*)$, $\varepsilon''(\omega,T) + \sigma_0(T)/(\omega\varepsilon_0) = -\mathrm{Im}(\varepsilon^*)$ and a concurrent measurement of σ_0.

Dielectric Relaxation of Bulk and Bound Water

The complex dielectric permittivity of bulk water within the TDR frequency range is well described by a single Debye relaxation process:

$$\varepsilon_{fw}^*(\omega,T)=\varepsilon_\infty+\frac{\varepsilon_{fws}(T)-\varepsilon_\infty}{1+j[\omega\tau_{fwc}(T)]} \quad [6]$$

where ε_{fws} is the static dielectric permittivity of bulk water, ε_∞ is the dielectric permittivity at infinite frequencies, and τ_{fwc} is the characteristic time scale of the relaxation process with relaxation frequency $\omega_c = 2\pi f_c = 1/\tau_{fwc}$. We used the empirical expressions of Stogryn (1971, 1995) to evaluate temperature-dependent ε_{fws} and τ_{fwc}, respectively, as

$$\varepsilon_{fws}(T)=\frac{3.70886\times10^4-82.168T}{4.21854\times10^2+T} \quad [7]$$

and

$$2\pi\tau_{fwc}(T)=1.1109\times10^{-10}-3.824\times10^{-12}T+6.938\times10^{-14}T^2-5.096\times10^{-16}T^3 \quad [8]$$

In contrast to bulk water, the rotational movements of water molecules adsorbed by or adjacent to the surfaces of soil minerals are dampened in the TDR frequency range, thereby reducing their polarizability and permittivity at the same temperature and electromagnetic field frequency. Reduced polarizability of bound water occurs only at high frequencies, beyond the lower frequency influence of proton hopping (Calvet, 1975; Hunt et al., 2006) and electrode polarization (Schwan, 1966). For these high frequencies, the time scale of reorientational motions of water molecules adsorbed by clays are one to four orders of magnitude greater than that for bulk liquid water. This results in a decline in ε' for water with a concomitant rise in $\varepsilon''(\omega)$ to a maximum value that occurs at a frequency equivalent to the inverse of the relaxation time (Sposito and Prost, 1982). The microscopic dielectric relaxation time τ of a polar molecule is usually interpreted in terms of the generalized Debye (1929) formula:

$$\tau=\frac{4\pi r^3\eta}{kT} \quad [9]$$

where r is the molecular radius (m), k is the Boltzmann constant (1.38065×10^{-23} J K^{-1}), η is dynamic viscosity, and T is absolute temperature (K). Low (1976) demonstrated that the mean viscosity of smectite gels was greater than that of bulk water and decreased exponentially with increasing water content. Using electron spin resonance spectroscopy, McBride and Baveye (1995) characterized the rotational relaxation times of the interlamellar water of smectite gels and showed that the results could be explained by an exponential increase in water viscosity toward the surface. Or and Wraith (1999) combined the Debye formula, Eq. [9], with a modified expression of Low (1976) to derive a characteristic relaxation time τ_{bwc} as a function of temperature and the distance from the surface x (nm):

$$\tau_{bwc}(x,T)=\frac{4\pi r^3c_0}{kT\exp\left[-\frac{1}{T}\left(\frac{b}{x}+d\right)\right]} \quad [10]$$

where $b = 162.1$ nm K, $d = 2.047\times10^3$ K, and $c_0 = 9.5\times10^{-7}$ Pa s^{-1} are constants used to describe the temperature dependency of the viscosity of bulk water. We take a similar approach as Or and Wraith (1999) except that, rather than assuming a constant permittivity of bound water based on a cut-off frequency, we use a Cole–Davidson modification of the Debye equation to calculate the geometric mean of the complex permittivity ε_{bw}^* within a region $0 < x \le \delta_{bw}$ normal to the surface:

$$\varepsilon_{bw}^*(\omega,T)=\exp\left(\frac{1}{\delta_{bw}}\int_0^{\delta_{bw}}\ln\left\{\varepsilon_\infty+\frac{\varepsilon_{fws}-\varepsilon_\infty}{[1+j\omega\tau_{bwc}(x,T)]^{\beta_{CD}}}\right\}dx\right) \quad [11]$$

where β_{CD} is the Cole–Davidson distribution parameter to account for a distribution of relaxation times skewed toward lower frequencies ($\beta_{CD} \le 1$). The thickness of the bound water layer, δ_{bw} (nm), is characterized by the specific surface area of clay A_s (m^2 g^{-1}), the soil bulk density ρ_b (kg m^{-3}), and the volumetric fraction of bound water θ_{bw} (m^3 m^{-3}):

$$\delta_{bw}=\frac{10^6\theta_{bw}}{A_s\rho_b} \quad [12]$$

The bound water fraction is defined as

$$\theta_{bw}=\begin{cases}\theta & \theta<\delta_L A_s\rho_b\times10^{-6}\\ \delta_L A_s\rho_b\times10^{-6} & \theta\ge\delta_L A_s\rho_b\times10^{-6}\end{cases} \quad [13]$$

where δ_L is the maximum thickness (nm) of the bound water region. A geometric mean is used to calculate the "effective" complex dielectric permittivity rather than the harmonic and arithmetic means, which delineate the upper and lower bounds, respectively.

The surface-induced increase in viscosity described above is only one of the mechanisms by which clays can restrict the rotational mobility of water molecules. Counterions in the diffuse double layer can also reduce static permittivity by the formation of hydrated shells of water molecules around the ions, with these molecules exhibiting restricted orientational polarizability (Sposito and Prost, 1982; Friedman et al., 2006). Hence, the

magnitude of nonpolarizable hydrated water molecules is determined by the surface charge density of the clay, the charge density of the cation, and the valency of the cation. These cation-specific effects are not explicitly accounted for in the physical model and hence the colloid surface area, A_s, should be considered a fitted parameter that depends on the mineralogy of the soil and, to a lesser extent, the dominant saturating cations.

Effective Frequency

The complex permittivity of bulk and bound water was formulated in the preceding equations as a function of the propagation of sinusoidal plane waves at a single frequency. Time domain reflectometry measures the propagation velocity of a broadband step voltage pulse with a rise time of ~200 ps and hence a bandwidth of approximately 1.75 GHz (Robinson et al., 2003). Due to the limitations of the connectors, TDR device, and coaxial cable, however, the effective bandwidth can be considerably reduced (Logsdon, 2000). Here, we take the approach that a single "effective" or centroid frequency, ω_R, representing the entire TDR bandwidth can be used to approximate the dielectric response of soils (Topp et al., 2000; Robinson et al., 2003, 2005). A principal difficulty with this approach is that signal attenuation during pulse propagation can filter out high-frequency components and shift the effective measurement bandwidth, thereby biasing the calculation of the apparent permittivity. This problem can be resolved by (i) measuring the bandwidth at the termination of the coaxial cable, and (ii) approximating the change in bandwidth resulting from frequency-dependent amplitude losses while traversing the TDR rod.

Pulse rise time is a convenient measurement of the degree of attenuation associated with the loss of high-frequency components in a time-domain pulse traversing a coaxial cable. The first-order response for a unit step input signal is

$$E(t)=1-\exp\left(\frac{-t}{\tau_c}\right) \qquad [14]$$

where t is time (s), E is relative voltage, and τ_c (s) is the mean transition duration of the pulse measured by an oscilloscope. Bandwidth can be approximated by fitting τ_c and the 100% amplitude level of the unit step function to the rise time of the reflection of the TDR pulse at the open termination of the coaxial cable. This method is equivalent to the 10 to 90% rise time calculation for a simple RC filter (Kaiser, 2005). By fitting the step response, however, it avoids some of the difficulties associated with identification of the 100% amplitude for signals filtered by lossy cables and in the presence of ringing and overshoot.

In Eq. [14], the measured transition duration consists of both the forward and reverse contributions to rise time. The overall (round-trip) rise time is the square root of the sum of the squares of the individual rise times (Electronic Industries Alliance, 1998). By setting the forward and reverse rise times as equivalent, application of the Electronic Industries Alliance (1998) definition results in an overall measured rise time, τ_c, equal to the single-pass rise time multiplied by $\sqrt{2}$. Consequently, the effective bandwidth of the pulse at the termination of the coaxial cable, ω_S (rad s^{-1}), is

$$\omega_S=\frac{\sqrt{2}}{\tau_c} \qquad [15]$$

In Eq. [15], the transition duration is divided by $\sqrt{2}$ to remove the rise time contribution of the return trip from the rise time recorded by the oscilloscope. Because ω_S is calculated based on the transition duration at the termination of the coaxial cable, it reflects a frequency associated with the transmission losses of the cabling and interconnects as well as the TDR instrument's pulse rise time. In an earlier study, Topp et al. (2000) recognized the value of incorporating a measurement of bandwidth into the calculation of the real and imaginary components of permittivity. They estimated an effective frequency based on the rise time of the second reflection associated with the termination of the TDR rod. This avoided the necessity of approximating the frequency-dependent amplitude loss during propagation through the soil. Rise-time measurements, however, are strictly applicable in the absence of significant dispersion (Hook et al., 2004). Consequently, evaluating the rise time based on the open termination reflection would appear impractical in fine-textured soils with significant phase velocity dispersion. Moreover, in practice, identifying the voltage associated with the 100% rise time is problematic when σ_0 is large (e.g., >0.1 S m^{-1}).

Most soils are dispersive to some degree, which causes broadening and phase delay of the electromagnetic pulse. Another source of pulse degradation is the attenuation of high-frequency components caused by absorption of the electromagnetic energy by the surrounding medium. Dissipative mechanisms such as electrical conduction and dielectric damping result in a decibel power loss proportional to the attenuation rate α (m^{-1}) for nonmagnetic materials (von Hippel, 1954), expressed as

$$\alpha(\omega)=\omega\left[\frac{\mu_0\varepsilon_0\varepsilon'}{2}\left(\sqrt{1+\tan^2\delta}-1\right)\right]^{1/2} \qquad [16]$$

where μ_0 is the vacuum magnetic permeability (1.257×10^{-6} H m^{-1}). For soils and many geologic materials, attenuation of the incident pulse is frequency dependent such that high-frequency components are attenuated preferentially over low-frequency components (Davis and Annan, 1989; Jol, 1995; Bano, 1996). This implies a downshift in the bandwidth as the pulse propagates through a lossy medium. Frequency-dependent attenuation originates from bulk and bound water polarization processes, and, at lower frequencies, from Maxwell–Wagner polarization (Chen and Or, 2006a) and surface polarization resulting from the tangential migration of counterions near the clay surface (Ishida et al., 2000).

Using a statistically based approach proposed by Dines and Kak (1979) and later used by Liu et al. (1998) for radar attenuation tomography, we derived an approximate expression that links the downshift in bandwidth to attenuation based on a knowledge of the input amplitude spectrum, $S(\omega)$, and an attenuation filter, $H(\omega)$. The propagation constant, γ (m^{-1}), for a plane wave in lossy dielectrics is $\gamma = \alpha + j\beta$, where the attenuation constant is α (Eq. [16]) and the phase constant is $\beta = (\omega/c)\sqrt{K_a}$. A decline in bandwidth occurs only when high-frequency components are attenuated preferentially over low-frequency components. Bandwidth reduction is therefore dependent on the real part of the propagation constant and is independent of the phase constant, which does not influence the amplitude and only causes a delay in signal propagation due to phase shift. Based on the time-independent telegraphers (plane wave) equation, signal amplitude along the propagation path ($2L$) decays exponentially

with distance (Kraus, 1992; Yanuka et al., 1988), and, consequently, the attenuation filter can be expressed as

$$H(\omega) = \exp\left[-\alpha(\omega)2L\right] \qquad [17]$$

As proposed by Liu et al. (1998) for radar attenuation tomography, the center or effective frequency of the attenuated pulse, ω_R, can be calculated based on the integral formula for the centroid of the amplitude spectrum

$$\omega_R = \frac{\int_0^\infty S(\omega)H(\omega)\omega \mathrm{d}\omega}{\int_0^\infty S(\omega)H(\omega)\mathrm{d}\omega} \qquad [18]$$

Here, we approximate the input amplitude spectrum at the termination of the cable using a third-order Butterworth filter (Paarmann, 2001):

$$S(\omega) = \sqrt{\begin{array}{l}\mathrm{Re}\left[\dfrac{\omega_S^3}{(s+\omega_S)(s^2+s\omega_S+\omega_S^2)}\right]^2 \\ +\mathrm{Im}\left[\dfrac{\omega_S^3}{(s+\omega_S)(s^2+s\omega_S+\omega_S^2)}\right]^2\end{array}} \qquad [19]$$

where $s = j\omega$. The third-order filter has a steeper amplitude roll-off compared with lower order filters and generates a spectrum for ω_S = 4 rad GHz (0.6 GHz) that has little amplitude (less than –42 dB) above 3 GHz, a region where nearly all of the measured signal in TDR oscilloscopes is noise (Friel and Or, 1999). A unique property of the third-order filter is that the centroid of the amplitude spectrum is equivalent to the cutoff or corner frequency. Consequently, when Eq. [18] is solved for the lossless case (α = 0), the resulting effective frequency $\omega_R = \omega_S$, the bandwidth of the input spectrum. The effective frequency of the pulse after it has propagated through the soil can be directly obtained by calculating the real and imaginary components of the bulk permittivity using the mixing models in Eq. [4] or [5] and inserting these values into Eq. [16] to calculate attenuation. This permits K_a to be estimated in Eq. [1] using the single-frequency approximation of $\omega = \omega_R$ in the dielectric mixing equations.

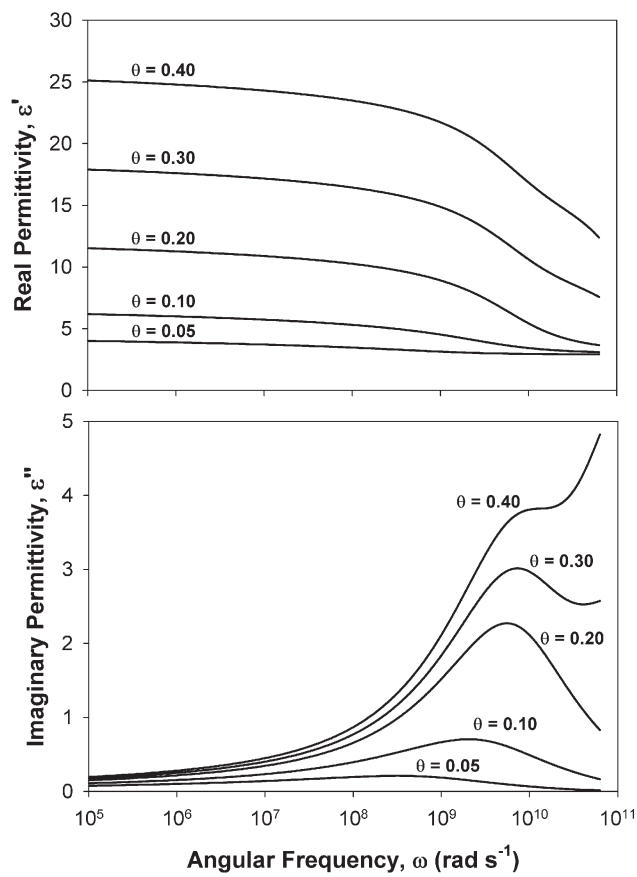

Fig. 1. Simulated dielectric dispersion and absorption curves using the power-law mixing model (without direct current conductivity contributions) across a range of water contents for a soil with a large surface area (A_s = 200 m^2 g^{-1}). For these calculations, bound water content θ_{bw} = 0.205 m^3 m^{-3} and, consequently, bulk water polarization at $\omega > 5 \times 10^{10}$ rad s^{-1} is evident only for volumetric water content $\theta > \theta_{bw}$. Parameters used in the simulation are provided in Table 1.

Bulk and bound water polarization characterized by Eq. [6] and [11], respectively, describe two distributions with relaxation frequencies $1/\tau_{bwc} \gtrsim 10^8$ rad s^{-1} (Fig. 1). The dielectric absorption curve of a single soil mineral consists of several overlapping polarization mechanisms extending from the 0.1 MHz to the GHz range (Ishida et al., 2000) and would be considerably more complex for soils with mixed mineralogy and a wide range of particle diameters (Logsdon, 2000). Although Eq. [11] may be satisfactory for estimating the dielectric response at a broadband step pulse centered around 1 GHz, uncertainties in the frequency distribution of polarization mechanisms may bias its use for estimating the frequency-dependent attenuation of a broadband pulse. An additional difficulty is that, in practice, a solution involving the numerical integration of Eq. [18] will be computationally expensive because water content must be determined iteratively using a root-finding algorithm.

Given the above-noted difficulties in estimating attenuation resulting from dielectric damping, we developed an alternative empirical approach to estimate the effective frequency without a specific knowledge of the dielectric absorption spectrum of the soil across a range of water contents. Assuming that the amplitude spectrum can be represented by an exponential probability distribution, that attenuation increases linearly with frequency, and that polarization losses increase with increasing soil water content, we derived an approximation for the effective frequency due to relaxation losses as (see Appendix)

$$\omega_R = \frac{\omega_{R1}(\omega_S)}{1+2LA\alpha_2\left[\omega_{R1}(\omega_S)\right]\left[\omega_{R1}(\omega_S)\right]^B} \qquad [20]$$

where A (s^B) and B are fitted empirical constants, $\omega_{R1}(\omega_S)$ is the effective frequency resulting from losses associated with bound water and other surface-related polarization mechanisms, and α_2 is the attenuation function associated with the polarization of bulk water evaluated as a function of frequency, $\omega_{R1}(\omega_S)$.

MATERIALS AND METHODS

Permittivity measurements of soil (34% clay) obtained from the Bt horizon of a Richfield silt loam (a fine, smectitic, mesic Aridic Argiustoll) and Ottawa sand (F110, U.S. Silica, Berkeley Springs, WV) were used to compare with model-calculated permittivities. The experimental procedures used to obtain these measurements and associated data are described in detail by Schwartz et al. (2009); therefore, we will repeat only the essential information here. A range of volumetric water contents for Ottawa sand and Richfield silt loam were obtained by thorough mixing with different ratios of water and packing the

mixture into 0.2-m diam. by 0.21-m-long polyvinyl chloride columns. For water contents >0.30 $m^3\ m^{-3}$, air-dry Richfield soil was packed into the columns, after which the soil was saturated from the bottom. In this case, water contents were adjusted through a combination of drainage and surface evaporation, after which the columns were sealed and permitted to come to equilibrium. Equilibrium was assumed to be attained when a negligible change in permittivity with time was recorded after a minimum of 1 wk. Trifilar probes (0.2-m length) were installed vertically into the prepared soil columns. Waveforms were acquired using a Tektronix 1502C cable tester (Tektronix, Beaverton, OR) and processed by a computer running the TACQ software (Evett, 2000a, 2000b). Electrical conductivity measurements were performed using the procedure of Castiglione and Shouse (2003) with cable-specific air and short-circuit reflection coefficients with probe constants calibrated in KCl solutions. Quadruplicate travel time and bulk electrical conductivity measurements were taken at room temperature (22–23°C), in a refrigerator (6–8°C), and in an incubator (40–42°C). The TDR measurements were completed after 2 d of equilibration under each temperature regime. Gravimetric water content was determined after each set of measurements.

Algorithms written in FORTRAN were used to calculate the apparent permittivity of the soil given the soil volumetric water content, temperature, bulk density, bulk electrical conductivity, and the bandwidth of the input spectrum, ω_S. The input bandwidth frequency was estimated by fitting the time constant and the 100% amplitude level to the open-ended reflection measured at the termination of the lead coaxial cable with the TDR probe removed (see Schwartz et al., 2009). Bulk electrical conductivity was estimated as

$$\sigma_0(T)=\sigma_{25}\left[\frac{\theta}{1-(\rho_b/\rho_s)}\right]^n[1+\Delta(T-298.15)] \qquad [21]$$

where σ_{25} is the bulk dc conductivity (S m^{-1}) at saturation and 25°C, n is a fitted empirical exponent, and Δ (K^{-1}) is a multiplier to account for the response of electrical conductivity to temperature above and below 25°C. We used an estimate of σ_0 given by Eq. [21] in the calculations rather than the actual measurement so that simulations would be continuous in the first derivative with respect to changes in water content and temperature. Constants and variables used to obtain all simulated results are provided in Table 1 except where otherwise indicated.

Based on the preceding theory, there are two approaches toward calculating the effective frequency of the soil: (i) an analytic solution of Eq. [2–13] to calculate attenuation across a range of frequencies in Eq. [16] and then estimate the effective frequency in Eq. [18]; or (ii) a direct approximation of the effective frequency using Eq. [20] with fitted parameters p, the polarization loss factor ($m^3\ m^{-3}$), and m, a dimensionless empirical coefficient. In both cases, the apparent permittivity is calculated equivalently by solving Eq. [2–13] to calculate the complex permittivity for the estimated effective frequency. The integral given in Eq. [11] to calculate the complex permittivity of bound water was evaluated using Gaussian quadrature. Integration of Eq. [18] was also performed using Gaussian quadrature with an upper limit of $20\omega_S$. An iterative procedure was used to calculate the apparent permittivity in connection with Method (ii) above because the direct approximation of the effective frequency using Eq. [20] requires that the real part of permittivity $\varepsilon'(\omega_R)$ be known vis a vis α_1 and α_2 in Eq. [A3] and [A8], respectively. The initial estimate of real permittivity was approximated using the empirical relationship between $\sqrt{K_a}$ and θ (Topp and Reynolds, 1998) given the low-loss approximation that $\varepsilon' \approx K_a$. Subsequently, the dielectric mixing model was solved with $\omega = \omega_R$ so the real and imaginary components of permittivity and hence the apparent permittivity in Eq. [1] could be calculated. Next, the updated value of real permittivity was substituted back into Eq. [20] to recalculate the effective frequency. This iterative procedure was continued until the change in the value of the apparent permittivity was less than a specified error. Typically, convergence was obtained within 10 iterations using an error tolerance of 10^{-10}. Because the analytic solution in Method (i) above involved the integration of attenuation across a range of frequencies, the execution time of this algorithm was nearly two orders of magnitude longer than the algorithm using the approximate solution Method (ii) for frequency decline.

RESULTS AND DISCUSSION

Introduction of the Cole–Davidson equation to account for a distribution of relaxation times and integrating this result across the bound water layer in Eq. [11] avoids the difficulties associated with identifying cutoff frequencies delineating rotationally hindered water (Or and Wraith, 1999). Moreover, this approach also permits an approximation of the frequency-dependent relationships for both the real and imaginary permittivity of bound water. Substitution of the complex permittivity of bound water into the power-law mixing model yields dielectric absorption curves (Fig. 1) similar in form to those measured by Ishida et al. (2000) in a dielectric spectroscopic study of montmorillonite and other pure clay mineral slurries. The intermediate-frequency process identified by Ishida et al. (2000) as associated with bound water has distribution peaks at frequencies of 10 to 30 MHz, about

Table 1. Notation, definitions, and default parameter values used in model simulations.

Parameter and value	Description
$a = 0.68$	Exponent for the power-law mixing model
$A_s = 200\ m^2\ g^{-1}$	Specific surface area of the soil
$L = 0.2$ m	Physical length of the time-domain reflectometry rod
$m = 1$	Exponent to describe the increase in polarization losses with water content
$n = 1.29$	Fitted exponent to describe the increase in bulk electrical conductivity with water content
$p = 20\ m^3\ m^{-3}$	Polarization loss factor describing dielectric losses due to bound water
$r = 0.25$ nm	Effective radius of water molecule
$T = 298.15$ K	Soil temperature
$\beta_{CD} = 1$	Cole–Davidson distribution parameter
$\Delta = 0.0232\ K^{-1}$	Multiplier to account for the response of the bulk electrical conductivity to temperature
$\delta_L = 0.75$ nm	Maximum thickness of the bound water region
$\varepsilon_\infty = 3.2$	Dielectric constant of bulk and bound water at infinite frequencies
$\varepsilon_a = 1.0$	Relative dielectric permittivity of air
$\varepsilon_s = 5.0$	Relative dielectric permittivity of soil solids
$\rho_b = 1350\ kg\ m^{-3}$	Bulk density of soil
$\rho_s = 2650\ kg\ m^{-3}$	Particle density of soil
$\sigma_{25} = 0.12\ S\ m^{-1}$	Bulk electrical conductivity of the soil at saturation and 25°C
$\omega_S = 2.85$ rad GHz	Input bandwidth estimated from rise time measurements

one order of magnitude lower than those exhibited in Fig. 1 at intermediate soil water contents. Permittivity spectra obtained by Logsdon (2005) for a moist loam soil lacked distribution peaks (>0.1 MHz), however, suggesting that for natural soils, there were probably several indeterminate relaxation processes that extended across a wide frequency range. Notwithstanding, above ~50 MHz (314 rad MHz) our predicted response of the real and imaginary permittivity to changes in soil water content are consistent with theory and detailed measurements (Wang, 1980; Spiridonov, 1982; Or and Wraith, 1999; Wagner et al., 2007). Real permittivity of the bound water increases with increasing soil water content until $\theta = \theta_{bw}$, reflecting an increase in the average polarizability of water molecules as the thickness of the bound water layer increases. Likewise, the average time constant associated with bound water polarization decreases with increasing water content, resulting in a shift in the distribution peaks (Fig. 1). Lastly, an increase in the imaginary permittivity with increasing frequency above the bound water relaxation frequency is realized only when $\theta > \theta_{bw}$, reflecting the shorter time constants of unbound water.

Because dc conductivity is partitioned from the mixing models in Eq. [4] and [5], interfacial polarization at the particle–solution interfaces (such as the Maxwell–Wagner effect) are not included in the model. Consequently, the strong frequency dependence of the real permittivity at frequencies <100 MHz (Ishida et al., 2000; Chen and Or, 2006a) is not simulated in Fig. 1. While Maxwell–Wagner-induced frequency dependence of the real permittivity has a negligible effect on the high-frequency determination of travel time from TDR waveforms, it can have a strong influence on dielectric sensors operating at low (<100 MHz) frequencies (Chen and Or, 2006b).

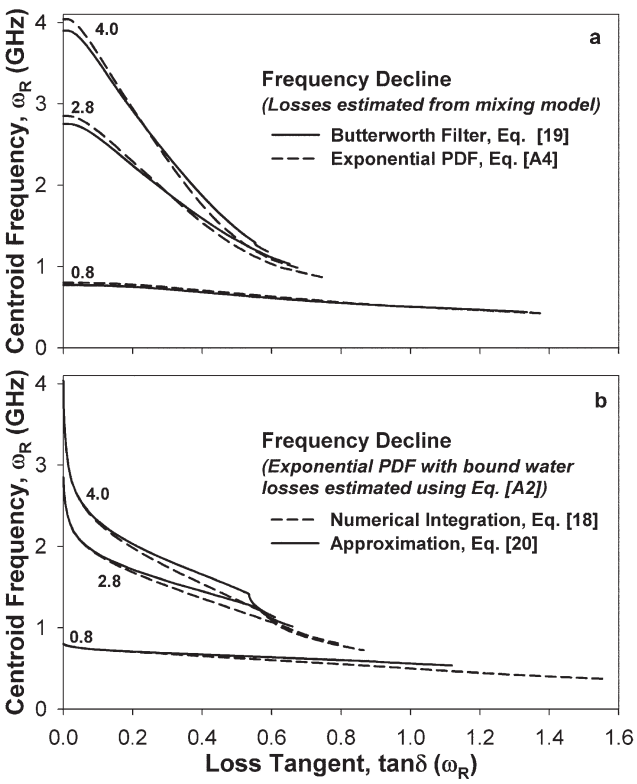

Fig. 2. Simulated frequency downshift for (a) polarization and ohmic losses calculated using the power-law mixing model Eq. [4] in conjunction with amplitude spectrums approximated using a third-order Butterworth filter or an exponential probability density function (PDF) and (b) polarization losses calculated using an empirical expression (polarization loss factor p = 10) in conjunction with an exponential PDF. Numbers adjacent to curves represent the bandwidth of the input amplitude spectrum, ω_S (GHz rad). A range of loss tangents was obtained by calculating real and imaginary permittivity across a range of soil water contents (0.0–0.45 m^3 m^{-3}) with bulk electrical conductivity calculated using Eq. [21] with exponent n = 1.6 and σ_{25} = 0.15 S m^{-1}. All other parameters used in the simulation are provided in Table 1.

The decline in effective frequency was calculated based on the change in the centroid of the amplitude spectrum using two methods: (i) losses were estimated using the dielectric mixing model and ω_R was obtained in conjunction with the integral expression of the centroid in Eq. [18]; or (ii) losses were estimated using Eq. [A2] and [A7], which permitted ω_R to be calculated using an approximate closed form solution in Eq. [20]. The two alternative solutions for three bandwidth spectra (ω_S) are illustrated in Fig. 2a and 2b, respectively, along with the simulated frequency declines demarcating potential errors with respect to the assumptions in deriving Eq. [20]. Use of an exponential probability density function (PDF) rather than the Butterworth amplitude spectrum (Fig. 2a) resulted in minor differences in the frequency decline at all bandwidths (ω_S = 0.8, 2.8, and 4.0 rad GHz) and was principally caused by the divergence in the roll-off between the two spectra. Simulation of the frequency decline using the integral expression of the centroid with the exponential PDF and bound water polarization losses calculated using Eq. [A2] (Fig. 2b, dashed line) shows that the approximate solution (Eq. [20]) slightly overestimates ω_R. This discrepancy results from a small frequency dependence of attenuation due to conductive effects and an underestimation of dielectric damping at larger loss tangents.

At an input bandwidth of ω_S = 2.85 rad GHz (454 MHz), an ~1.8 rad GHz (287 MHz) decline in effective frequency was simulated for the range of solutions (Fig. 2). The generated range in effective frequencies compares closely to those measured in the Topp et al. (2000) and Logsdon (2000) studies (100–500 MHz). The greatest declines were attained at high water contents corresponding to the largest loss tangents. The steep frequency decline at low water contents exhibited in Fig. 2b arises because of the assumption that polarization losses increase linearly with increasing water contents (m = 1 in Eq. [A2]). Setting the exponent to larger m values (e.g., m = 1.6) results in a more gradual decline in the effective frequencies with respect to the loss tangent (not shown). At an input bandwidth of ω_S = 0.80 rad GHz (127 MHz), both approaches yielded analogous and small declines in effective frequency because most of the frequency-dependent attenuation is centered above 1 GHz (Fig. 1). All solutions exhibited a proportionately smaller decline in frequency from soil water contents ranging from θ_{bw} to saturation compared with the air dry to θ_{bw} range. At $\theta > \theta_{bw}$, ε' increases at a greater rate than ε'' with increasing water content, resulting in little or no change in frequency-dependent attenuation with increasing water content.

It is instructive to consider the predicted response of the apparent permittivity with regard to the effect of the ohmic and dielectric losses incorporated into the dielectric mixing model.

Setting $\mathrm{Im}(\varepsilon_{bw}^*) = 0$ results in an underestimation of K_a at all water contents (Fig. 3). Moreover, including $\mathrm{Im}(\varepsilon_{bw}^*)$ in the solution diminishes the effect of bound water on the overall permittivity of the soil. Although bound water has a lower permittivity than bulk water, which results in a lower apparent permittivity of the soil, dielectric damping will partly offset this reduction because of its contribution to the loss tangent and frequency-dependent attenuation. Ignoring bulk electrical conductivity will also result in an underestimation of the apparent permittivity. Conductive losses will tend to be more important in fine-textured soils because dielectric damping associated with bound water causes a significant decline in frequency, which in turn increases the contribution of conductive effects to the loss tangent. If complex dielectric permittivity is solved without considering the decline in effective frequency during propagation, apparent permittivity is again underestimated. For specific surface areas ranging from 150 to 300 $m^2\ g^{-1}$, the simulations suggest that ignoring loss mechanisms or the associated decline in effective frequency results in a 5 to 22% underestimation of the apparent permittivity, with errors increasing with increasing surface area. Accordingly, loss mechanisms need to be considered in conjunction with the decline in bandwidth during signal propagation through fine-textured soils.

Solving for apparent permittivity using the two mixing models with an effective frequency calculated by either the analytic Eq. [18] or empirical Eq. [20] approach yields a set of four solutions (Fig. 4). All four models gave reasonable fits to the measured apparent permittivity for the Bt horizon of the Richfield soil across the entire soil water content range. Based on the simulated results for a range of specific surface areas, however, it is apparent that the apparent permittivity was more closely predicted using a smaller surface area for the de Loor–Dobson model compared with the power-law model. At soil water contents near saturation, the solutions calculated using Eq. [16] for attenuation tend to converge across a wide range of specific surface areas. Such an outcome results from the magnitude of the apparent permittivity being dependent on the opposing effects of the loss tangent and the real part of permittivity, especially at high soil water contents.

Or and Wraith (1999) demonstrated that the response of apparent permittivity to temperature was positive for soils with significant (e.g., >70 $m^2\ g^{-1}$) specific surface areas and negative for coarse-textured soils. They attributed this phenomenon to the interplay between the temperature dependencies of the static dielectric constant of water and the volumetric fraction of bound water in the soil. Such a response is evident in Fig. 5 for the measured apparent permittivities of the Richfield loam and Ottawa sand. Both simulated and measured results suggest a strong linear trend, with the absolute value of the slope increasing with increasing soil water contents. Differences between measured and simulated slopes were not significant ($P = 0.95$) except for the set of measurements recorded at $\theta = 0.280\ m^3\ m^{-3}$. Simulated temperature responses for the other prospective solutions (Fig. 4) are similar (not shown). These results suggest that the model performed well at predicting the temperature responses based on the equations used to calculate the relaxation frequencies for both bound and bulk water.

In contrast to Or and Wraith (1999), our measurements and simulations for the Richfield clay loam exhibit a positive response of apparent permittivity with respect to temperature at high soil water contents, with the bound water fraction comprising only half of the soil water. Or and Wraith (1999, Fig. 5b), however, measured an opposite trend at high water contents for the Millville silt loam: a declining apparent permittivity with increasing temperatures. Using the surface area and $\sigma_0(T)$ data for the Millville silt loam (Or and Wraith, 1999; Wraith and Or, 1999) and a polarization factor $p = 10$ to account for a lower clay content, our simulated results for both of the mixing models (Fig. 6) exhibit negative responses that compare closely to the measured results of Or and Wraith (1999). The capability of our simulations to predict both decreasing and increasing permittivity with increasing temperature at high soil water contents arises as a result

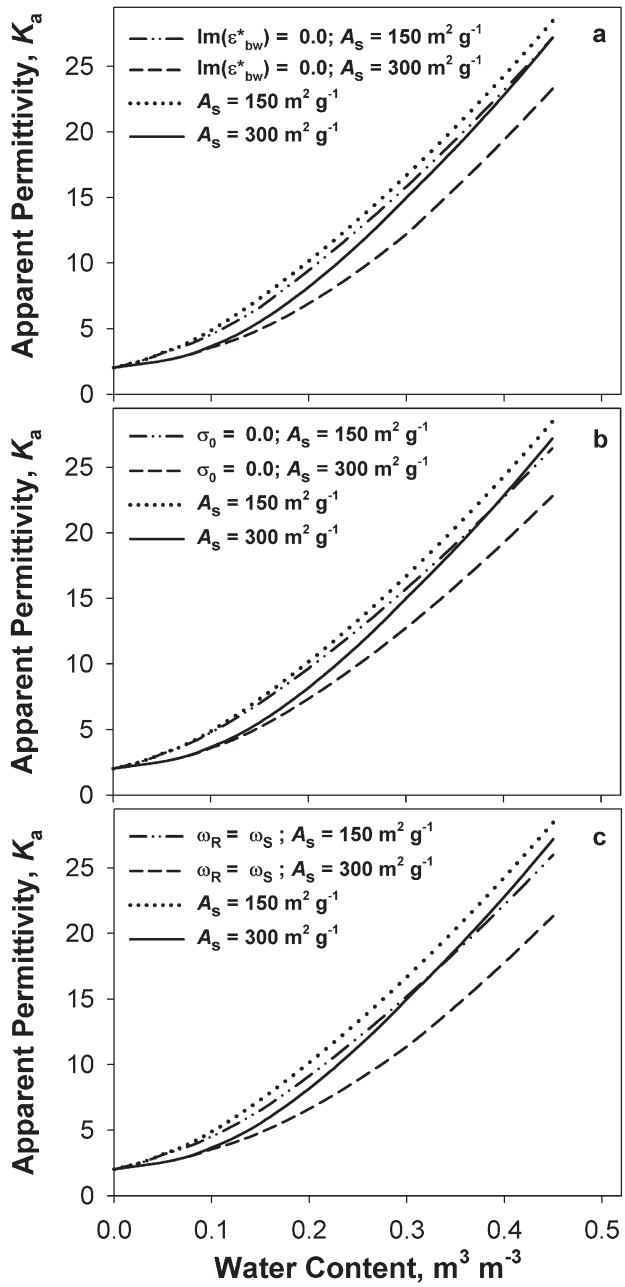

Fig. 3. Predicted apparent permittivity using the power-law mixing model compared with simulations ignoring losses due to (a) bound water polarization, (b) bulk electrical conductivity, or (c) frequency decline. Effective frequency ω_R was calculated using Eq. [18] with a Butterworth amplitude spectrum, and $\mathrm{Im}(\varepsilon_{bw}^*)$ is the imaginary part of the permittivity of bound water. All other parameters used in the simulation are specified in Table 1.

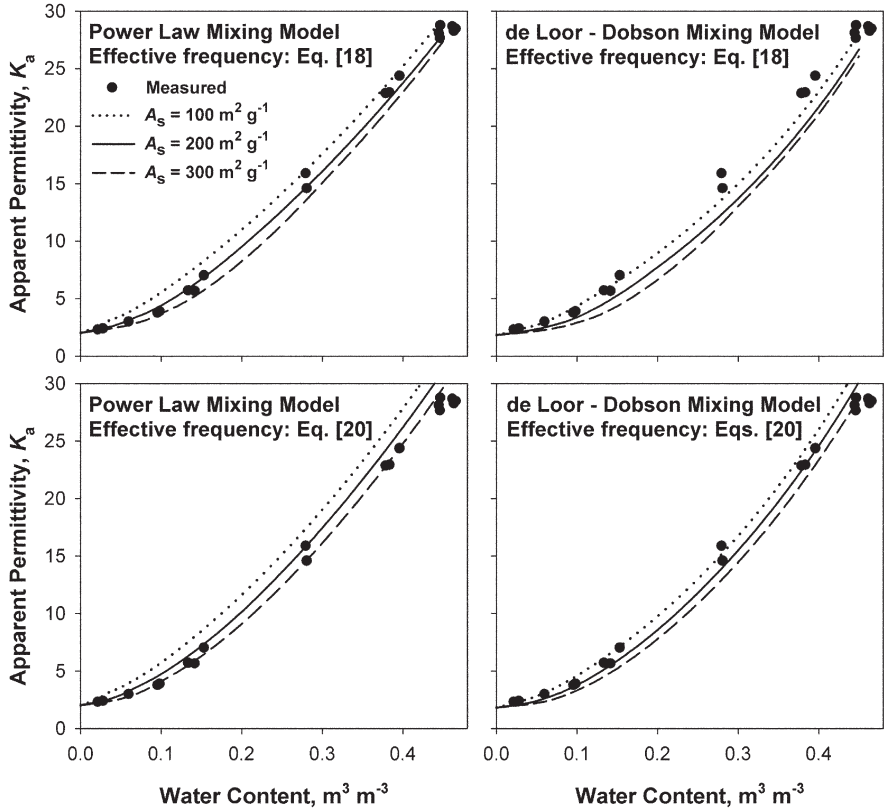

Fig. 4. Measured (Richfield soil Bt horizon) and simulated apparent permittivities for a range of specific surface areas using the power-law and the de Loor–Dobson mixing models. The amplitude spectrum used in conjunction with Eq. [18] was described by a Butterworth filter. Parameters used in the simulation are provided in Table 1.

of the inclusion of dielectric damping and ohmic losses in the calculation of the apparent permittivity, neither of which were considered significant in the earlier work. In addition, the decline in effective frequency during propagation will also tend to magnify the conductivity effect on apparent permittivity. Omitting ohmic losses in the solution obtained for the Richfield clay loam (Fig. 5) results in a positive temperature response at $\theta = 0.151$ and 0.280 m^3 m^{-3}, a flat response at $\theta = 0.384$ m^3 m^{-3}, and a negative response at $\theta = 0.445$ m^3 m^{-3} (not shown). The predicted influence of dielectric damping of bound and bulk water on the response of apparent permittivity is considerably more complex, but will generally be negative except at low (e.g., $\theta < 0.1$ m^3 m^{-3}) volumetric soil water contents. Obviously, ohmic and dielectric damping losses have a significant influence on the temperature response of apparent permittivity for the Richfield clay loam. The smaller clay content of the Millville silt loam (17%) will result in considerably lower ohmic losses which, at high soil water contents, are insufficient to offset the decline in the static dielectric constant with increasing temperature. These results demonstrate that loss mechanisms and declines in effective frequency will need to be considered to accurately predict the soil water content of fine-textured soils across a range of temperatures.

SUMMARY AND CONCLUSIONS

We developed and evaluated a physically based algorithm to estimate the real and imaginary components of the complex dielectric permittivity using a four-phase dielectric mixing formula with bulk electrical conductivity evaluated separately. The model was also used to predict frequency-dependent attenuation and a single "effective" frequency approximation of the apparent permittivity of the soil. The modeled response of the apparent permittivity to changes in temperature is caused by the temperature dependence of relaxation times for bulk and bound water as well as measured or simulated bulk electrical conductivity.

Above 50 MHz, the modeled responses of the real and imaginary permittivity to changes in soil water content were consistent with theory and detailed measurements in the literature. Using a centroid frequency downshift method, signal bandwidth was predicted to decline from 450 MHz (2.85 rad GHz) to about 160 MHz (1.0 rad GHz) with increasing soil water contents. Frequency decline for an input bandwidth of 130 MHz (0.80 rad GHz) was negligible, reflecting that modeled polarization mechanisms with relaxation frequencies >100 MHz were responsible for most of the frequency-dependent attenuation. For specific surface areas ranging from 150 to 300 m^2 g^{-1}, simulations indicate that ignoring dielectric and conductive losses or the associated decline in effective frequency results in a 5 to 22% underestimation of the apparent permittivity. Both the power-law and de Loor–Dobson mixing models gave a reasonable approximation to the measured apparent permittivity for a silty clay loam (34% clay) across the entire soil water content range. Moreover, modeled results were able to describe the behavior of apparent permittivity in response to temperature for two soils with contrasting bulk electrical conductivity contributions to losses. This demonstrates that the thermodielectric response of fine-textured soils comes about from the interplay among the temperature dependencies of the static permittivity of bulk water, the volumetric fraction of bound water, and the bulk electrical conductivity. Conductive effects on the temperature response are obviously strongly tied to the effective measurement frequency. These results demonstrate that loss mechanisms and declines in the effective frequency will need to be considered to accurately predict the soil water content of fine-textured soils across a range of temperatures and bulk electrical conductivities normally encountered in field settings.

Although preliminary tests of this model suggest that it can describe the response of apparent permittivity to changes in soil water content across a range of temperatures, input bandwidths, and clay contents (Schwartz et al., 2009), model robustness will depend on the suitability of some of the assumptions. Representation of polarization using only two relaxation frequencies (bulk and bound water) is a crude simplification of an actual soil system. Although additional polarization mechanisms could be included, it is not clear if inclusion of these additional parameters would significantly improve the estimates of apparent permittivity. Our analysis has also as-

sumed that a single "effective" frequency can be used to predict the broadband dielectric response of the soil and this frequency can be approximated by calculating plane-wave attenuation across a range of frequencies with an amplitude spectrum described by a third-order Butterworth filter. Evidence supporting these assumptions is incomplete and will require further investigation.

Despite the difficulties discussed above, we believe that measurements of soil temperature, bulk electrical conductivity, bulk density, and input bandwidth in conjunction with travel time measurements and soil-specific calibrations can improve the accuracy of soil water content evaluations in the field. Besides the measurements noted above, model calibration would entail the fit of the specific surface area, the exponent for the power-law mixing formula, and an additional one to two parameters depending on the effective frequency equation chosen. Such a small number of fitting parameters is desirable and is in the range of the number of fitted parameters typically used in purely empirical equations. In addition, computational requirements of the algorithm are modest such that the solution would be amenable to routine field use and inversion required for estimating water content from travel time measurements.

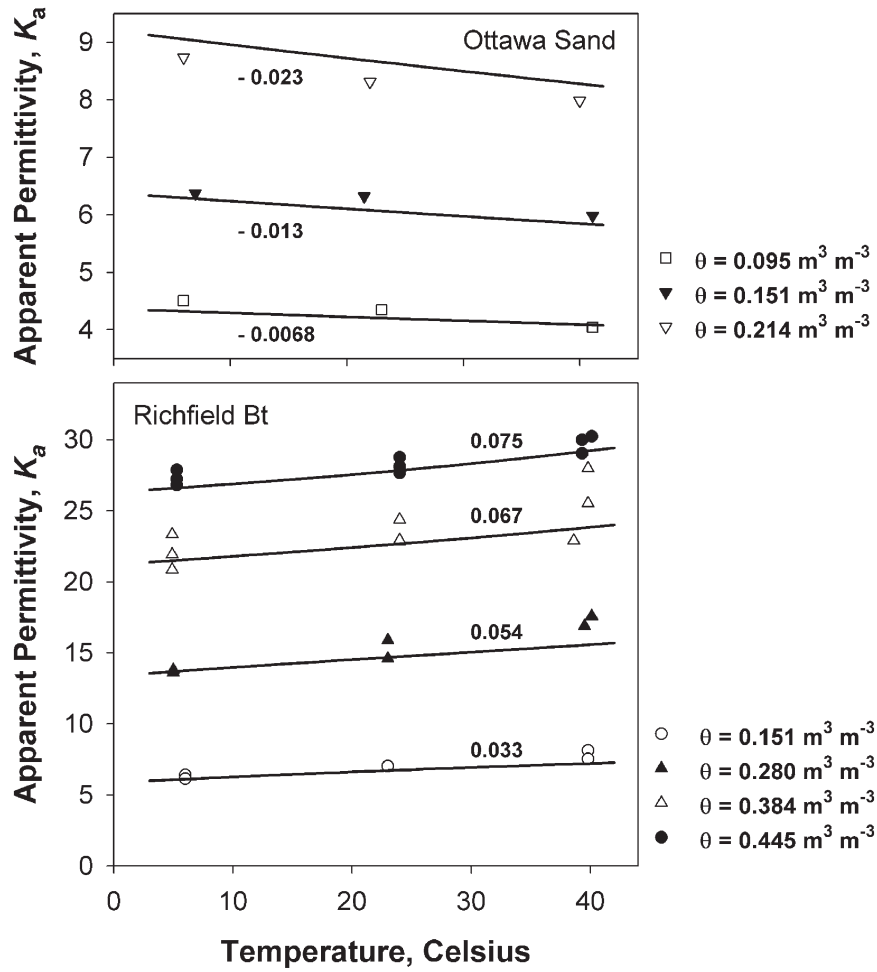

Fig. 5. Measured (symbol) and simulated (line) response of apparent permittivity to soil temperature across a range of water contents (θ) using the power-law mixing model. A specific surface area of A_s = 250 m^2 g^{-1} and a polarization loss factor p = 20 were used to simulate the response of the Richfield soil Bt horizon. For the Ottawa sand, A_s = 0.0, p = 0.0, power-law exponent a = 0.45, bulk density ρ_b = 1680 kg m^{-3}, relative permittivity of sand ε_s = 2.5, input bandwidth ω_S = 4.0 rad GHz (637 MHz), and σ_{25} = 0.012 S m^{-1} were used in the simulations. All other parameters used in the simulation are provided in Table 1. Each symbol at a given temperature represents a replicate column measurement. Numbers adjacent to predicted responses are slopes (°C^{-1}).

APPENDIX

Numerical integration of Eq. [18] can be computationally demanding for practical situations where large data sets are to be processed to inversely estimate water contents from apparent permittivity measurements. Such a rigorous approach may be unnecessary considering the uncertainties in the description of the frequency distribution of polarization mechanisms for a soil calculated using the mixing models. Here we seek a closed-form approximation of the effective frequency specified in Eq. [18]. Substitution of Eq. [3] into Eq. [16] and taking the first-order binomial approximation of $[(1 + \tan^2 \delta)^{1/2} - 1]$ yields a low-loss ($\tan \delta < 0.5$) approximation for the attenuation factor:

$$\alpha(\omega) = \frac{\omega}{2}\left\{\mu_0\varepsilon_0\varepsilon'(\omega)\left[\frac{\varepsilon''(\omega)+(\sigma_0/\omega\varepsilon_0)}{\varepsilon'(\omega)}\right]^2\right\}^{1/2} \quad [A1]$$

Setting the imaginary part of permittivity $\varepsilon'' = 0$ in Eq. [A1] demonstrates that, on simplification, attenuation resulting from conductive effects is nearly independent of frequency under low-loss conditions (Chen and Huang, 1998). Consequently, ohmic losses attenuate the signal to the same extent across the entire spectrum (Friel and Or, 1999), which results in no high-frequency filtering and no change in bandwidth.

Detailed spectroscopic studies of mineral soil water systems show that the imaginary part of the complex dielectric permittivity increases with increasing water content (Saarenketo, 1998; Logsdon, 2005). Here we make a simple assumption that the aggregate imaginary permittivity resulting from bound water polarization can be approximated as

$$\varepsilon''_{\text{bwsoil}}(\omega) = p\theta^m \quad [A2]$$

where p is a fitted polarization loss factor (m^3 m^{-3}) and m is a dimensionless empirical coefficient. Because of the involvement of colloid surface area in the magnitude of dielectric damping, p would be expected to increase with increasing clay content. Substitution of Eq. [A2] into Eq. [A1] and ignoring conductive effects yields

$$\alpha_1(\omega) \approx \frac{\omega p \theta^m}{2}\sqrt{\frac{\mu_0\varepsilon_0}{\varepsilon'(\omega)}} \quad [A3]$$

which results in attenuation $\alpha_1(\omega)$ linearly increasing with frequency, characteristic of the frequency response in low-loss geo-

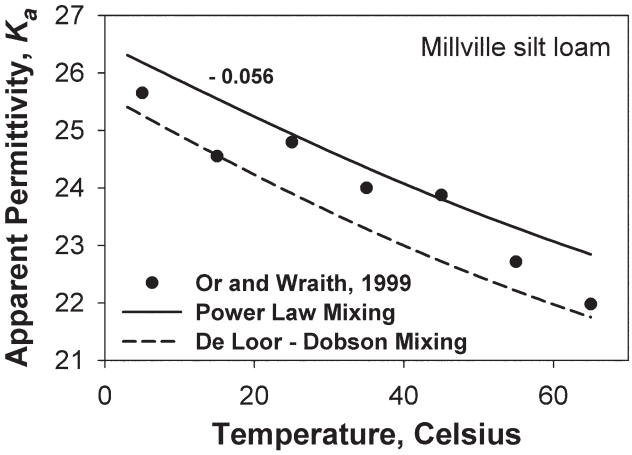

Fig. 6. Measured (Or and Wraith, 1999) and simulated temperature response of apparent permittivity for a Millville silt loam at a volumetric water content of 0.419 m^3 m^{-3}. Effective frequency was calculated using Eq. [20] with an input bandwidth ω_S = 2.7 rad GHz (430 MHz) and polarization loss factor p = 10. Bulk electrical conductivity data presented by Wraith and Or (1999) were approximated using Eq. [21] with σ_{25} = 0.063 S m^{-1}, exponent n = 1.29, and $\triangle$ = 0.0225 K^{-1}. Surface area (A_s = 73 m^2 g^{-1}), bulk density (ρ_b = 1270 kg m^{-3}) and the power-law exponent (a = 0.60) used in the simulations are as per Or and Wraith (1999). All other parameters used in the simulations are provided in Table 1. Numbers adjacent to predicted responses are slopes (°C^{-1}).

logic materials (Turner and Siggins, 1994; Noon et al., 1998). Such an approximation, termed the *constant Q model*, permits the evaluation of ground-penetrating radar signals independent of frequency.

An approximate representation of the amplitude spectrum can be obtained using the exponential PDF, a one-parameter, continuous distribution written as

$$S(\omega)=\frac{1}{\omega_S}\exp\left(\frac{-\omega}{\omega_S}\right) \qquad [A4]$$

where ω_S is the mean of the distribution as well as the angular frequency of the pulse at the termination of the coaxial cable. Analogous to the third-order Butterworth filter (Eq. [19]) when the integral expression Eq. [18] is solved for the lossless case using the exponential distribution, the resulting effective frequency $\omega_R = \omega_S$. The exponential distribution has a roll-off similar to the Butterworth filter down to –40 dB amplitude, after which it declines more steeply. Substitution of the attenuation expression $\alpha_1(\omega)$ into Eq. [17] and solving for the integrals in Eq. [18] using the exponential distribution (Eq. [A4]) with the assumption that the real part of permittivity is constant with respect to frequency yields a closed-form solution by Laplace transform for the effective frequency approximation of the attenuated pulse ω_{R1}:

$$\omega_{R1}(\omega_S)=\frac{\omega_S}{1+2L\alpha_1(\omega_S)} \qquad [A5]$$

with an input spectral bandwidth of ω_S.

In soils with significant amounts of clays, the decline in frequency will be dominated by polarization processes related to bound water. Hence, under these conditions, Eq. [A5] is a good approximation of the effective frequency. In low-surface-area soils, however, bulk water polarization can also cause a significant shift in frequency (e.g., Friel and Or, 1999), especially when short, low-loss coaxial cables are used. The imaginary part of the complex permittivity of bulk water can be written as (Or and Wraith, 1999)

$$\varepsilon_{fw}''=\frac{\omega\tau_{fwc}(\varepsilon_{fws}-\varepsilon_\infty)}{1+\omega^2\tau_{fwc}^2} \qquad [A6]$$

Attenuation resulting from bulk water polarization can be approximated by first assuming that $\omega^2\tau_{fwc}{}^2 \approx 0$ within the TDR frequency range. With this approximation, substitution of Eq. [A6] into Eq. [4] and solving for the imaginary part of permittivity with the assumption that all other imaginary components in the mixing model are negligible yields

$$\varepsilon_{fwsoil}''\approx\omega\tau_{fwc}\theta_{fw}^{1/a}(\varepsilon_{fws}-\varepsilon_\infty) \qquad [A7]$$

where ε_{fwsoil}'' is an estimate of the composite imaginary permittivity of the soil considering only the dielectric damping losses of bulk water. Substituting this result for the imaginary permittivity in Eq. [A1] and, as before, ignoring conductive losses yields

$$\alpha_2(\omega)\approx\frac{\omega^2\tau_{fwc}}{2}\sqrt{\mu_0\varepsilon_0\frac{\theta_{fw}^{2/a}(\varepsilon_{fws}-\varepsilon_\infty)^2}{\varepsilon'}} \qquad [A8]$$

for the low-loss approximation of attenuation in soils due to bulk water polarization.

Similar to the attenuation given by Eq. [A3], the effective frequency of the attenuation given in Eq. [A8] can be solved by Laplace transform; however, because of the ω^2 term, integration yields an exponential × complementary error function expression (Abramowitz and Stegun, 1972) that is numerically unstable. Within the TDR bandwidth of interest (600–3600 rad MHz 96–573 MHz), the frequency shift for dielectric damping losses of bulk water can be approximated by fitting an expression analogous to Eq. [A5] to numerically integrated results calculated for bulk water relaxation losses (Eq. [A6]) to give

$$\omega_{R2}=\frac{\omega_S}{1+2LA\alpha_2(\omega_S)\omega_S^B} \qquad [A9]$$

where $A = 7.442 \times 10^5\ s^{-0.5904}$ and $B = -0.5904$ are fitted constants. Using the t-shifting theorem for Laplace transforms, substitution of Eq. [A5] solved for ω_S into Eq. [A9] yields the closed-form approximation for the frequency shift due to bulk and bound relaxation losses as given in Eq. [20].

ACKNOWLEDGMENTS

We gratefully acknowledge Sally Logsdon and Guy Serbin for the helpful exchanges and reviews of an earlier version of this manuscript. Alan Schlegel kindly provided samples of the Richfield loam for use in the study. In addition, special thanks are extended to Amanda McCarthy for her assistance in the laboratory and with waveform collection.

REFERENCES

Abramowitz, M., and I.A. Stegun. 1972. Handbook of mathematical functions. Natl. Bureau of Standards, Appl. Math. Seri. 55. U.S. Gov. Print. Office, Washington, DC.

Bano, M. 1996. Constant dielectric losses of ground-penetrating radar waves. Geophys. J. Int. 124:279–288.

Birchak, J.R., C.G. Gardner, J.E. Hipp, and J.M. Victor. 1974. High dielectric constant microwave probe for sensing soil moisture. Proc. IEEE 62:93–98.

Boyarskii, D.A., V.V. Tikhonov, and N.Yu. Komarova. 2002. Model of

dielectric constant of bound water in soil for applications of microwave remote sensing. J. Electromagnetic Waves Appl 16:411–412.

Calvet, R. 1975. Dielectric properties of montmorillonite saturated by bivalent cations. Clays Clay Miner. 23:257–265.

Castiglione, P., and P.J. Shouse. 2003. The effect of ohmic cable losses on time-domain reflectometry measurements of electrical conductivity. Soil Sci. Soc. Am. J. 67:414–424.

Chen, H.-W., and T.-M. Huang. 1998. Finite-difference time-domain simulation of GPR data. J. Appl. Geophys. 40:139–163.

Chen, Y., and D. Or. 2006a. Geometrical factors and interfacial processes affecting complex dielectric permittivity of partially saturated porous media. Water Resour. Res. 42:W06423, doi:10.1029/2005WR004744.

Chen, Y., and D. Or. 2006b. Effects of Maxwell–Wagner polarization on soil complex dielectric permittivity under variable temperature and electrical conductivity. Water Resour. Res. 42:W06424, doi:10.1029/2005WR004590.

Davis, J.L., and A.P. Annan. 1989. Ground-penetrating radar for high-resolution mapping of soil and rock stratigraphy. Geophys. Prospect. 3:531–551.

Debye, P. 1929. Polar molecules. Dover Publ., Mineola, NY.

de Loor, G.P. 1968. Dielectric properties of heterogeneous mixtures containing water. J. Microw. Power 3–2:67–73.

Dines, K.A., and A.C. Kak. 1979. Ultrasonic attenuation tomography of soft tissues. Ultrason. Imaging 1:16–33.

Dirksen, C., and S. Dasberg. 1993. Improved calibration of time domain reflectometry soil water measurements. Soil Sci. Soc. Am. J. 57:660–667.

Dobson, M.C., F.T. Ulaby, M.T. Hallikainen, and M.A. El-Rayes. 1985. Microwave dielectric behavior of wet soil: II. Dielectric mixing models. IEEE Trans. Geosci. Remote Sens. 23:35–46.

Electronic Industries Alliance. 1998. Rise time degradation test procedure for electrical connectors, sockets, cable assemblies or interconnection systems. Electronic Industries Alliance Standard TP-102.

Evett, S.R. 2000a. The TACQ program for automatic time domain reflectometry measurements: I. Design and operating characteristics. Trans. ASAE 43:1939–1946.

Evett, S.R. 2000b. The TACQ program for automatic time domain reflectometry measurements: II. Waveform interpretation methods. Trans. ASAE 43:1947–1956.

Evett, S.R., J.A. Tolk, and T.A. Howell. 2005. Time domain reflectometry calibration in travel time, bulk electrical conductivity, and effective frequency. Vadose Zone J. 4:1020–1029.

Friedman, S.P., S.B. Jones, and D.A. Robinson. 2006. Plenary lecture: Review of geometrical and interfacial factors determining effective permittivity–volumetric water content relationships of soils and rocks. Pap. 48. *In* Proc. TDR 2006: Int. Symp. and Worksh. on Time Domain Reflectometry for Innovative Soils Applications, 3rd, West Lafayette, IN. 17–20 Sept. 2006. Available at engineering.purdue.edu/TDR/Papers/48_Paper.pdf. College of Eng., Purdue Univ., West Lafayette, IN.

Friel, R., and D. Or. 1999. Frequency analysis of time-domain reflectometry (TDR) with application to dielectric spectroscopy of soil constituents. Geophysics 64:707–718.

Heimovaara, T.J., W. Bouten, and J.M. Verstraten. 1994. Frequency domain analysis of time domain reflectometry waveforms: 2. A four-component complex dielectric mixing model for soils. Water Resour. Res. 30:201–209.

Hook, W.R., T.P.A. Ferré, and N.J. Livingston. 2004. The effects of salinity on the accuracy and uncertainty of water content measurements. Soil Sci. Soc. Am. J. 68:47–56.

Hook, W.R., and N.J. Livingston. 1995. Propagation velocity errors in time domain reflectometry measurements of soil water. Soil Sci. Soc. Am. J. 59:92–96.

Hunt, A.G., S.D. Logsdon, and D.A. Laird. 2006. Percolation treatment of charge transfer in humidified smectite clays. Soil Sci. Soc. Am. J. 70:14–23.

Ishida, T., T. Makino, and C. Wang. 2000. Dielectric-relaxation spectroscopy of kaolinite, montmorillonite, allophane, and imogolite under moist conditions. Clays Clay Miner. 48:75–84.

Jol, H.M. 1995. Ground penetrating radar antennae frequencies and transmitter powers compared for penetration depth, resolution and reflection continuity. Geophys. Prospect. 43:693–709.

Kaiser, K.L. 2005. Electromagnetic compatibility handbook. CRC Press, Boca Raton, FL.

Kraus, J.D. 1992. Electromagnetics. 4th ed. McGraw-Hill, New York.

Liu, L., J.W. Lane, and Y. Quan. 1998. Radar attenuation tomography using the centroid frequency downshift method. J. Appl. Geophys. 40:105–116.

Logsdon, S.D. 2000. Effect of cable length on time domain reflectometry calibration for high surface area soils. Soil Sci. Soc. Am. J. 64:54–61.

Logsdon, S.D. 2005. Soil dielectric spectra from vector network analyzer data. Soil Sci. Soc. Am. J. 69:983–989.

Logsdon, S.D., and D.A. Laird. 2004. Electrical conductivity spectra of smectites as influenced by saturating cation and humidity. Clays Clay Miner. 52:411–420.

Low, P.F. 1976. Viscosity of interlayer water in montmorillonite. Soil Sci. Soc. Am. J. 40:500–505.

McBride, M.B., and P. Baveye. 1995. Mobility of anion spin probes in hectorite gels: Viscosity of surficial water. Soil Sci. Soc. Am. J. 59:388–394.

Mironov, V.L., M.C. Dobson, V.H. Kaupp, S.A. Komarov, and V.N. Kleshchenko. 2004. Generalized refractive mixing dielectric model for moist soils. IEEE Trans. Geosci. Remote Sens. 42:773–785.

Noon, D.A., G.F. Stickley, and D. Longstaff. 1998. A frequency-independent characterization of GPR penetration and resolution performance. J. Appl. Geophys. 40:127–137.

Or, D., and J.M. Wraith. 1999. Temperature effects on soil bulk dielectric permittivity measured by time domain reflectometry: A physical model. Water Resour. Res. 35:371:383.

Paarmann, L.D. 2001. Design and analysis of analog filters: A signal processing perspective. Springer Publ., Princeton, NJ.

Robinson, D.A., S.B. Jones, J.M. Wraith, D. Or, and S.P. Friedman. 2003. A review of advances in dielectric and electrical conductivity measurement in soils using time domain reflectometry. Vadose Zone J. 2:444–475.

Robinson, D.A., M.G. Schaap, D. Or, and S.B. Jones. 2005. On the effective measurement frequency of time domain reflectometry in dispersive and nonconductive dielectric materials. Water Resour. Res. 41:WR02007, doi:10.1029/2004WR003816.

Roth, K., R. Schulin, H. Flühler, and W. Attinger. 1990. Calibration of time domain reflectometry for water content measurements using a composite dielectric approach. Water Resour. Res. 26:2267–2273.

Saarenketo, T. 1998. Electrical properties of water in clay and silty soils. J. Appl. Geophys. 40:73–88.

Schwan, H.P. 1966. Alternating current electrode polarization. Biophysik 3:181–201.

Schwartz, R.C., S.R. Evett, and J.M. Bell. 2009. Complex permittivity model for time domain reflectometry soil water content sensing: II. Calibration. Soil Sci. Soc. Am. J. 73:888–899 (this issue).

Spiridonov, V.I. 1982. A relaxation model for the dielectric properties of water in heterogeneous mixtures. Izmer. Tekh. 5:68–70.

Sposito, G., and R. Prost. 1982. Structure of water adsorbed on smectites. Chem. Rev. 82:553–573.

Stogryn, A.P. 1971. Equations for calculating the dielectric constant of saline water. IEEE Trans. Microw. Theory Tech. 19:733–736.

Stogryn, A.P. 1995. The microwave permittivity of sea and fresh water. GenCorp Aerojet, Azusa, CA.

Topp, G.C., J.L. Davis, and A.P. Annan. 1980. Electromagnetic determination of soil water content: Measurements in coaxial transmission lines. Water Resour. Res. 16:574–582.

Topp, G.C., and W.D. Reynolds. 1998. Time domain reflectometry: A seminal technique for measuring mass and energy in soil. Soil Tillage Res. 47:125–132.

Topp, G.C., S. Zegelin, and I. White. 2000. Impacts of real and imaginary components of relative permittivity on time domain reflectometry measurements in soils. Soil Sci. Soc. Am. J. 64:1244–1252.

Turner, G., and A.F. Siggins. 1994. Constant *Q* attenuation of subsurface radar pulses. Geophysics 59:1192–1200.

von Hippel, A.R. (ed.). 1954. Dielectric materials and applications. MIT Press, Cambridge, MA.

Wagner, N., E. Trinks, and K. Kupfer. 2007. Determination of the spatial TDR-sensor characteristics in strong dispersive subsoil using 3D-FEM frequency domain simulations in combination with microwave dielectric spectroscopy. Meas. Sci. Technol. 18:1137–1146.

Wang, J.R. 1980. The dielectic properties of soil–water mixtures at microwave frequencies. Radio Sci. 15:977–985.

Wraith, J.M., and D. Or. 1999. Temperature effects on soil bulk dielectric permittivity measured by time domain reflectometry: Experimental evidence and hypothesis development. Water Resour. Res. 35:361–369.

Yanuka, M., G.C. Topp, S. Zegelin, and W.D. Zebchuk. 1988. Multiple reflection and attenuation of time domain reflectometry pulses: Theoretical considerations for applications to soil and water. Water Resour. Res. 24:939–949.